Available online at www.sciencedirect.com
ScienceDirect
Construction and Building Materials 21 (2007) 1709–1719
Construction and Building MATERIALS
www.elsevier.com/locate/conbuildmat

Strength and serviceability performance of beams reinforced with GFRP bars in flexure

Biswarup Saikia, Phanindra Kumar, Job Thomas, K.S. Nanjunda Rao, Ananth Ramaswamy *

Department of Civil Engineering, Indian Institute of Science, Bangalore, India

Received 5 May 2005; received in revised form 11 February 2006; accepted 31 May 2006
Available online 20 September 2006

Abstract

Glass fiber reinforced polymer (GFRP) rebars have been identified as an alternate construction material for reinforcing concrete during the last decade primarily due to its strength and durability related characteristics. These materials have strength higher than steel, but exhibit linear stress–strain response up to failure. Furthermore, the modulus of elasticity of GFRP is significantly lower than that of steel. This reduced stiffness often controls the design of the GFRP reinforced concrete elements. In the present investigation, GFRP reinforced beams designed based on limit state principles have been examined to understand their strength and serviceability performance. A block type rotation failure was observed for GFRP reinforced beams, while flexural failure was observed in geometrically similar control beams reinforced with steel rebars. An analytical model has been proposed for strength assessment accounting for the failure pattern observed for GFRP reinforced beams. The serviceability criteria for design of GFRP reinforced beams appear to be governed by maximum crack width. An empirical model has been proposed for predicting the maximum width of the cracks. Deflection of these GFRP rebar reinforced beams has been predicted using an earlier model available in the literature. The results predicted by the analytical model compare well with the experimental data.

Keywords: GFRP; Flexure; Crack width; Deflection

1. Introduction

Earlier research works by Nawy and Neuwerth [1], Theriault and Benmokrane [2] Saadatmanesh and Ehsani [3], Shapira and Bank [4], Nanni [5], Yost et al. [6] Razaqpur et al. [7] and Kumar et al. [8] on utilization of glass fiber reinforced polymer (GFRP) rebar have indicated that it could be a promising material as an alternative to the conventional steel reinforcement in concrete structures. Presently, codes of practice (CSA S806 [9], ACI 440 [10], JSCE [11] and design guidelines – Sonobe et al. [12]) are available for practicing engineers to design and construct FRP reinforced concrete structures. The GFRP rebar have relatively high tensile strength and better resistance against corrosion in moist environments when compared to the conventional steel reinforcement [5]. However, GFRP rebars are brittle, which imposes a restriction on it being stressed to its failure limit. To avoid possible catastrophic failures, generally GFRP reinforced beams are designed using working stress design principles. In the present study, an attempt has been made to study the strength and serviceability performance of flexure critical concrete beams reinforced with GFRP rebar, which are designed based on limit state principles.

Nawy and Neuwerth [1] showed that the sectional analysis model used for concrete beams reinforced with steel rebars predicted the moment capacity of the concrete beams reinforced with GFRP rebar. Theriault and Benmokrane [2] studied on the strength, cracking behavior and deflection behavior of the concrete beams reinforced with FRP reinforcements. The strength of the concrete

* Corresponding author. Tel.: +91 80 2293 2817/2360 8850; fax: +91 80 2360 0404/2360 0683.
E-mail address: ananth@civil.iisc.ernet.in (A. Ramaswamy).

0950-0618/$ - see front matter © 2006 Elsevier Ltd. All rights reserved.
doi:10.1016/j.conbuildmat.2006.05.021

beam reinforced with FRP rebar was computed by plane-section analysis, in which the strain in concrete was set to 0.0035. Saadatmanesh and Ehsani [3] studied the behavior of concrete beams reinforced with GFRP rebar. At failure of the beams, debonding of GFRP rebar was not observed in this study. The research works of Shapira and Bank [4] indicated that FRP rebar is an alternate for conventional steel reinforcement in RC beams. The life-cycle cost of the FRP reinforced concrete beams has been computed and was found to be less than the corresponding cost of beams with conventional steel rebar. Nanni [5] proposed analytical models to compute the strength of concrete beams reinforced with FRP rebar. In these models the concrete is set to attain the failure strain and the strain in the reinforcement was limited to a maximum value corresponding to the failure strain in the rebar. Yost et al. [6] studied the strength and deflection of concrete beam reinforced with FRP rebar. The rotation of a block of concrete and the debonding of longitudinal reinforcement resulting in the anchorage failure were observed in the test program. The beams with FRP rebar failed at a load of 46–70% of their flexural capacity. The flexural capacity of the beam was computed by sectional analysis in which the rebar is assumed to maintain perfect bond with the surrounding concrete. Razaqpur et al. [7] proposed an analytical model for computing the deflection of concrete beams reinforced with FRP rebar. The model utilizes a tri-linear variation for the moment-curvature response of the beam. In all these works, the longitudinal reinforcement is assumed to be perfectly bonded to the surrounding concrete at failure.

In the present study, beams reinforced with GFRP rebar were cast using two different grades of concrete (65 MPa and 35 MPa) and tested. Control beams with longitudinal steel rebar were also cast and tested and the results are compared with the corresponding GFRP reinforced beams. The experimental study conducted by Xiao et al. [13] on the bond behavior of FRP with concrete indicated that the bond shear stress of FRP is as low as 1.287 MPa. The low modulus of elasticity of GFRP rebar resulting in relatively large deformations and smooth surface characteristics of the GFRP rebar leading to debonding type of failures, are important in determining the serviceability performance of GFRP reinforced beams. Hence, the serviceability constraints (cracking and deflection) generally will control the design of the GFRP reinforced beam sections. In the present study, an empirical model has been proposed for predicting the maximum width of the crack at various loading stages. An attempt has also been made to predict the deflection of the GFRP reinforced beams using models proposed in the literature (Razaqpur et al. [7]). Based on the present study, an analytical model has been proposed to estimate the ultimate strength of GFRP reinforced beams accounting for the slip between rebars and concrete as observed in the experiments. The predicted information such as ultimate strength, crack width and deflection has been compared with the corresponding experimental results and has been reported in this paper.

2. Experimental program

2.1. Details of beam specimens tested

A total of 10 beams of cross sectional dimension 180 mm width and overall height 250 mm were cast and tested under four-point bending. All the beams were tested over a clear span of 1340 mm. The shear span was maintained constant (420 mm) as shown in Fig. 1. The cross sectional details and loading arrangement of the test beams have also been presented in Fig. 1. All the beams were designed as singly reinforced sections based on the limit state principles.

In the first phase of the experimental program, five beams were cast with moderately high strength concrete (65 MPa) and tested. Out of the five beams, one had conventional steel reinforcement and the remaining four had GFRP rebar as longitudinal reinforcement. Among the four GFRP reinforced beams, one had plain concrete matrix and steel stirrups; the second one had plain concrete matrix and GFRP stirrups, the third had polymer modified fiber reinforced concrete (FPC) matrix and steel stirrups and the fourth beam had polymer modified fiber reinforced concrete (FPC) matrix and GFRP stirrups. Epoxy based GFRP rebar were used to reinforce the beams in this phase. The five beams in this phase were designed for an ultimate load of 290 kN.

In the second phase of the test program, five beams were cast with normal strength concrete (35 MPa). Out of these five beams, two had conventional steel reinforcement and other three had GFRP rebar as longitudinal reinforcement. One of the beams with longitudinal steel reinforcement had plain concrete matrix and steel stirrups while the other had GFRP stirrups and fiber reinforced concrete matrix. Of the three GFRP reinforced beams, one had plain concrete matrix and steel stirrup, the second one had fiber reinforced concrete and GFRP stirrup and the third beam had fiber reinforced concrete matrix and steel stirrups. As a substantial decrease was seen in the compressive strength of the concrete due to the addition of polymers in the first phase of the experimental program, a combination of fibers and polymers was not included in the second phase. Polyester based GFRP rebar were used to reinforce the beams in the second phase. The five beams in this phase were designed for an ultimate load of 225.0 kN.

The beams were designated to indicate its type (Flexure-F), the type of longitudinal reinforcement (steel-S, GFRP-G), the phase of the study (Phase I-1 corresponding to 65 MPa strength concrete and Phase II-2 corresponding to 35 MPa strength concrete), the type of transverse reinforcement (steel-S, GFRP-G) and the type of concrete used (ordinary concrete-OC, fiber reinforced concrete – FC and polymer modified fiber reinforced concrete – FPC). Thus FS1SOC indicates a flexure critical beam with steel as longitudinal reinforcement cast and tested in Phase-I (with moderately high strength concrete of 65 MPa) having steel stirrups and plain concrete matrix. The designations and the details of the test beam have been given in Table 1.

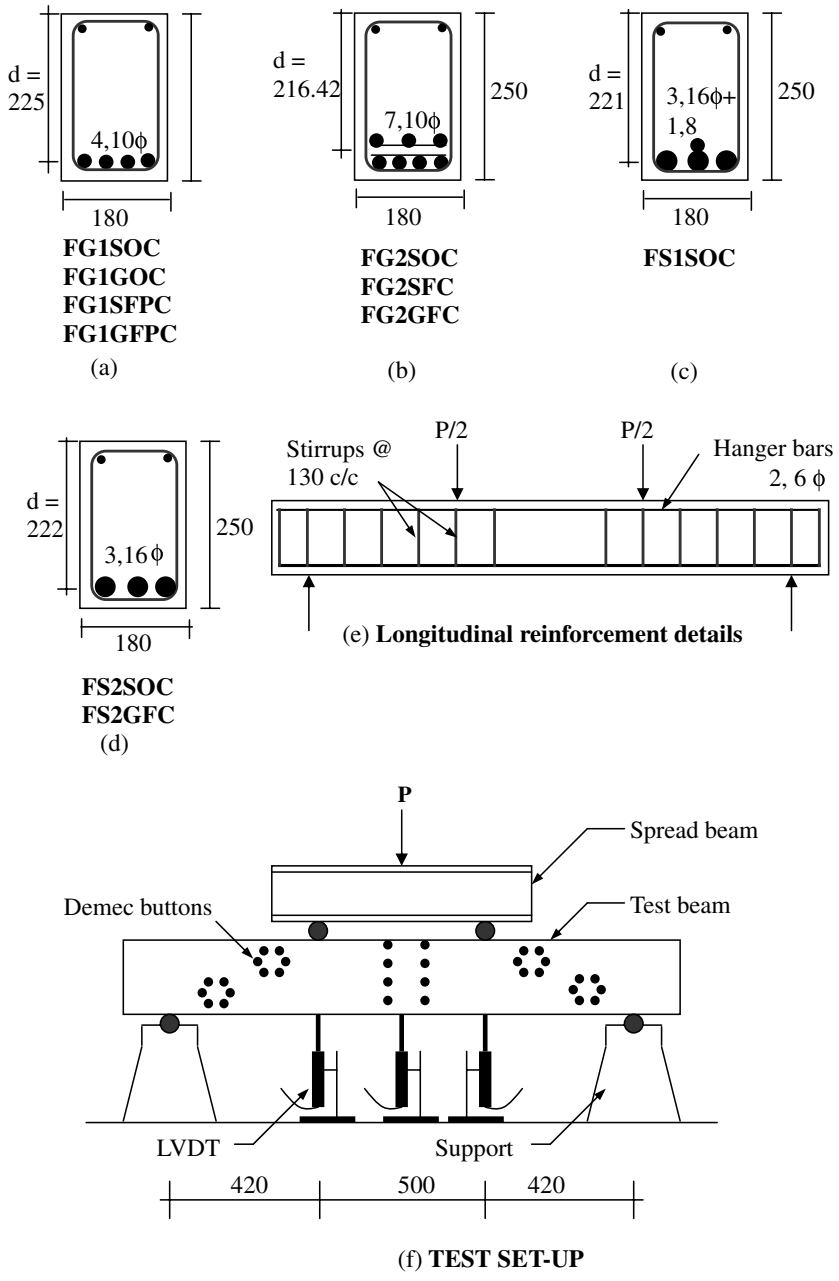

Fig. 1. Details of test beam and loading arrangement.

2.2. Materials and mix proportion

The constituent materials used in the concrete for casting of beams were cement, fine aggregate, coarse aggregate, fibers, polymer and water. Blended type cement with a specific gravity of 3.15 was used for casting the beam. Natural river sand of fineness modulus 2.32 was used as fine aggregate. Crushed stones having maximum aggregate size of 20 mm was used as coarse aggregate. Polypropylene fibers of 20 mm long were used at 0.1% by weight of the cement to prepare the fiber reinforced concrete. Styrene butadiene rubber was used at 10% by weight of cement along with the polypropylene fibers to prepare polymer modified fiber reinforced concrete. Sulponated naphthalene based super plasticiser was used for moderately high strength concrete mixes at a dosage of 0.54% of cement weight. The details of the mix proportion used for different test beams are given in Table 2.

Two types of GFRP rebar were used in the present study. GFRP rebar having an ultimate tensile strength (f_{gu}) of 971 MPa had 66.67% glass fibres and embedded in epoxy matrix. Similarly GFRP bars having an ultimate tensile strength of 466 MPa had 67.77% of glass fibers embedded in polyester matrix. The difference in strength of the two types of GFRP rebar was mainly due to the variation in strength of the binding matrix in the rebar. The matrix strength greatly influences the bond shear stress of

Table 1
Details of beam specimens tested

Sl. no.	Beam designation	Type of rebar	Longitudinal reinforcement[a]	Transverse reinforcement[a] (2-legged rectangular stirrup)	Companion cube strength f_{cu} (MPa)
Moderately high strength concrete (65 MPa) – Phase I					
1	FS1SOC	Steel	3, 16∅ + 1, 8∅	8∅ @ 130 c/c	65.23
2	FG1SOC	GFRP Epoxy	4, 10∅	8∅ @ 130c/c	67.77
3	FG1GOC		4, 10∅	G[b] @ 130c/c	63.84
4	FG1SFPC		4, 10∅	8∅ @ 130c/c	44.92
5	FG1GFPC		4, 10∅	G[b] @ 130c/c	39.26
Normal strength concrete (35 MPa) – Phase II					
6	FS2SOC	Steel	3, 16∅	8∅ @ 130c/c	42.28
7	FS2GFC		3, 16∅	G[b] @ 130c/c	37.82
8	FG2SOC	GFRP polyester	7, 10∅	8∅ @ 130c/c	41.82
9	FG2SFC		7, 10∅	8∅ @ 130c/c	38.26
10	FG2GFC		7, 10∅	G[b] @ 130c/c	38.26

[a] All dimensions are in mm.
[b] GFRP stirrup as shown in Fig. 3.

Table 2
Details of the concrete mix for the test beams

Sl. no.	Beam designation	Mix proportion W:C:FA:CA[a]	Additives		
			Super plasticiser	Fibres	Polymers
		by weight	% by weight of cement		
1	FS1SOC	0.37:1:1.09:1.45	0.54	–	–
2	FG1SOC			–	–
3	FG1GOC			–	–
4	FG1SFPC			0.1	10
5	FG1GFPC			0.1	10
6	FS2SOC	0.50:1:2.3:3.25	–	–	–
7	FS2GFC			0.1	–
8	FG2SOC			–	–
9	FG2SFC			0.1	–
10	FG2GFC			0.1	–

[a] W = water, C = cement, FA = fine aggregate and CA = coarse aggregate.

the discrete fibers. Though the fiber content is relatively high, the matrix strength is sensitive to the rebar rupture because the contribution of the fiber in load sustenance is a function of matrix strength (weakest link). Both types of GFRP used had approximately the same modulus of elasticity and were available in the form of 10 mm diameter bars. The experimental study of Orozco and Maji [14] and Thiagarajan [15] indicated that the surface treatments on smooth FRP rebar is essential to develop adequate bond in FRP reinforced concrete beams. Hence in the present study, two numbers of 2 mm diameter glass fiber strands dipped in epoxy were helically wound around the smooth 10 mm diameter GFRP rebar through a secondary manufacturing process to improve the bond with concrete as shown in Fig. 2. The tension test result of the steel and GFRP rebar used in the present study has been reported in Table 3.

Two legged closed loop steel stirrups and GFRP stirrups of rectangular cross section as shown in Fig. 3 were used as transverse reinforcement. The GFRP stirrups were prepared by cutting a GFRP rectangular tube made by filament winding process and cut to the width of 25 mm. The required width of the GFRP stirrups was computed by equating the shear resistance to that offered by an 8 mm ∅ 2-legged steel stirrup based on strength criteria. The strength and elastic properties of the GFRP stirrup strips have been given in Table 3.

2.3. Casting and testing of beams

One electrical resistance strain gauge capable of measuring ±20,000 micro-strains was mounted at the mid-span of the central longitudinal reinforcement and protective waterproofing coating was applied over it. All the longitu-

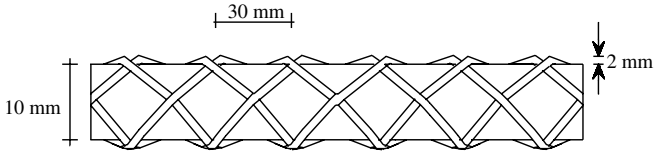

Fig. 2. Sketch of surface deformation with 2 mm ∅ GFRP strand on 10 mm ∅ rebar.

Table 3
Tension test result for different rebar

Rebar/stirrup material	Tension test			
	Modulus of elasticity MPa	Yield strength (MPa)	Ultimate tensile strength (MPa)	Ultimate tensile strain
Mild Steel (6 mm ∅)	195,000	262	280	0.032600
Deformed Steel (8 and 16 mm ∅)	189,800	440	557	0.038200
GFRP Epoxy (G1)	49,000	–	972	0.019854
GFRP Polyester (G2)	49,620	–	464	0.009370
GFRP strip (stirrup)	13,310	–	205	0.015420

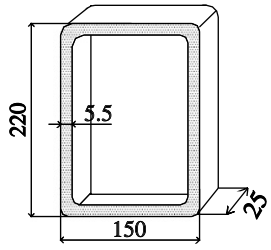

Fig. 3. Geometrical details of GFRP stirrup.

dinal reinforcements were placed in the mould with a clear cover of 20 mm for the bottom layer and sides. The constituent materials were weigh-batched and mixed using a rotating drum mixer. The fresh homogeneous mix was poured into the moulds and compacted using a needle vibrator. The sides of the mould were removed after 24 h of casting and wrapped with moist burlap for curing. After 28 days of moist curing, beams were white washed and surfaces were prepared to mount the demec points/electrical strain gauges. The demec points were mounted at the mid span and shear span (in the form of rosette) to measure the strain at various locations (Fig. 1(f)). The strains were measured using demec gauges having a least count of 1.57×10^{-5} strains. In addition, three numbers of wire type electrical strain gauges (range ±5000 micro-strains) were mounted on the rear face of the beam to measure the concrete surface strains. Deflection in the beam was measured using LVDT's at mid span and at the location of the loading points as shown in Fig. 1(f). The loading set-up of the test beams is shown in Fig. 1(e). Load was applied in increments of 50 kN. At each increment of load, concrete surface strains, deflections, width of the cracks and propagation of the cracks were recorded. The loading was stopped when the inclined crack formed in the shear span reached the top compression fiber leading to rebar pullout and failure.

3. Analytical model

The slip of the rebar and the block type rotation of cracked concrete have been observed at ultimate stage of loading of the GFRP reinforced beams. Hence load in these beams did not reach the designed ultimate value. Accounting for this fact, a model has been proposed for predicting the ultimate strength of the GFRP reinforced beams. In addition, prediction of the serviceability requirements such as crack width and deflection of the GFRP reinforced beams has also been attempted.

3.1. Prediction of beam strength accounting for the slip of rebar

Based on the experimental observations, the critical crack in the GFRP reinforced beams has been assumed to be inclined at 45 degrees with respect to the longitudinal axis as shown in Fig. 4. This crack initiated at a distance equal to effective depth of the beam '*d*' from the point of application of the load in the shear span of the beam. Strength of the beam has been computed by analyzing a critical section corresponding to a stage at which slip of the rebar is significant because beyond this stage, stress build up in the rebar is negligible (Fig. 5). The limiting strain in the rebar at stage where slip governs the failure of the beam ($\varepsilon_{\text{b-slip}}$) has been computed using Eq. (1).

$$\varepsilon_{\text{b-slip}} = \frac{\tau_b L_d (\pi \phi_b)}{E_b (\pi \phi_b^2/4)} \tag{1}$$

where L_d is the anchorage length of the rebar as shown in Fig. 4, τ_b is the maximum value of the average bond shear strength of the FRP rebar from the pullout test data shown in Fig. 5, ϕ_b is the diameter of the rebar and E_b is the modulus of elasticity of rebar as given in Table 3. From the Fig. 4, the anchorage length L_d of the GFRP rebar has been computed and is equal to (shear span + bearing − cover − effective depth).

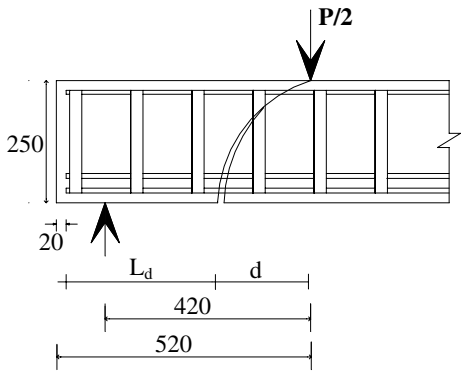

Fig. 4. Development length in GFRP reinforced beam.

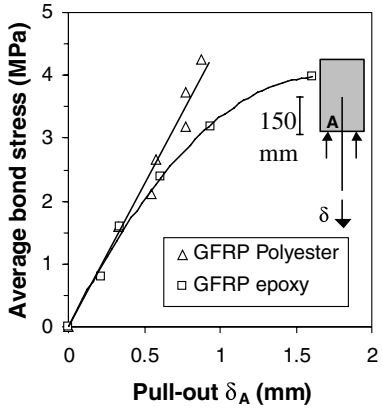

Fig. 5. Pullout test data of GFRP rebar.

The strain in the concrete at depth x_i from the extreme compression fiber (ε_{ci}) in the cross section of the beam was calculated using Eq. (2)

$$\varepsilon_{ci} = \frac{\varepsilon_{\text{b-slip}}}{(d_b - x_u)}(x_u - x_i) \tag{2}$$

where d_b and x_u are the effective depth and the depth of neutral axis from extreme compression fiber, respectively. In the presents study, d_b has been taken as the distance from the extreme compression fiber to the centroid of the layer of longitudinal rebar closest to the tension face of the beam section (d_{s3} in Fig. 6) and is computed as (overall depth − clear cover to longitudinal reinforcement − 0.5 × diameter of the bar).

As shown in Fig. 6, a linear variation of strain has been assumed along the depth of the cross-section of the beam. As proposed in IS 456 [16], the stress in concrete under compression has been assumed to be parabolic in the initial portion (up to a strain of 0.002) and constant beyond. The total compressive force offered by the concrete block is calculated using Eq. (3).

$$C_c = -\begin{cases} \frac{2}{3} f_{cu}\left[2\frac{\varepsilon_{cc}}{0.002} - \left(\frac{\varepsilon_{cc}}{0.002}\right)^2\right] b x_u; & \text{for } 0 \leqslant \varepsilon_{cc} \leqslant 0.002 \\ \frac{2}{3} f_{cu}\left(\frac{0.002}{\varepsilon_{cc}} x_u\right) b + f_{cu}\left(x_u - \frac{0.002}{\varepsilon_{cc}} x_u\right) b; & \text{for } 0.002 \leqslant \varepsilon_{cc} \leqslant 0.0035 \\ 0.00; & \text{if } \varepsilon_{cc} \geqslant 0.0035 \end{cases} \tag{3}$$

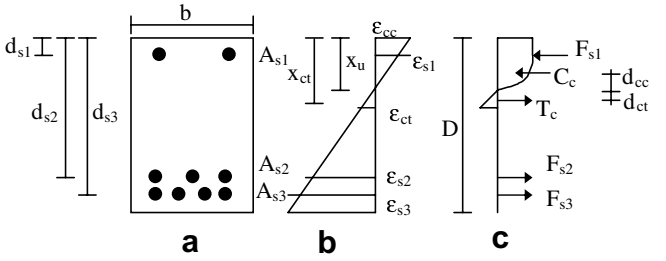

Fig. 6. Stress–strain variation along the depth of cross-section: (a) beam section, (b) concrete strain variation and (c) concrete stress variation and component forces.

f_{cu} in Eq. (3) is the cube compressive strength of concrete determined by testing the companion cube specimens. ε_{cc} in Eq. (3) is the strain at the extreme compression fiber, which is computed from Eq. (2) by substituting $x_i = 0$. 'b' is the width of the section.

The tension contribution of the concrete has been considered up to the cracking stage and the post cracking softening part of the tensile behavior of the concrete has been neglected. Also, the presence of polypropylene fibers has been ignored in tensile and compressive stress–strain properties. A linear variation has been assumed for the pre-cracking tensile stress–strain curve and the total tensile force due to the uncracked part of the concrete below the neutral axis (T_c) has been computed using Eq. (4)

$$T_c = \frac{1}{2} f_{ct}(x_{ct} - x_u) \tag{4}$$

$$f_{ct} = 0.7\sqrt{f_{cu}} \tag{5}$$

$$\varepsilon_{ct} = f_{ct}/E_{ct} \tag{6}$$

$$E_{ct} = E_c/2 \tag{7}$$

$$E_c = 5000\sqrt{f_{cu}} \tag{8}$$

f_{ct} in Eq. (4) is the tensile strength of concrete and is computed using Eq. (5), the prediction model proposed in IS 456. x_{ct} in Eq. (4) is the depth of the concrete from the extreme compression face at which cracking occurs and has been computed using Eq. (2) by substituting $\varepsilon_{ci} = \varepsilon_{ct}$. f_{cu} in Eq. (5) is the cube compressive strength of concrete and average compressive strength of the companion cubes tested has been presented in Table 1. ε_{ct} is the strain in concrete at cracking and has been computed using Eq. (6). E_{ct} in Eq. (6) is the initial tangent modulus of concrete in tension and has been computed using Eq. (7), originally proposed by Zhuang et al. [17]. E_c is the initial tangent modulus of concrete in compression and has been computed using Eq. (8), the model proposed in IS 456 [16].

The force contribution of the longitudinal reinforcements (F_{si}) has been computed using Eq. (9)

$$F_{si} = f_{si} A_{si} \tag{9}$$

where f_{si} and A_{si} are the stress in the rebar and area of the rebar, respectively. A sectional analysis has been carried out to compute the beam strength corresponding to a stage where bar slip governs the failure of the beam. The stress in the rebar f_{si} has been obtained from test data of the stress–strain plots shown in Fig. 7. The strains in the rebar at ith layer in the cross section has been assumed to be equal to the strain in surrounding concrete and has been computed using Eq. (2) by substituting appropriate values of depth of the layer from extreme compression fiber x_i. Splitting crack along the longitudinal reinforcement into the shear span (towards the support) formed at ultimate stage. Thus, the reduction in the embedded length of longitudinal rebar due to the formation of splitting crack has not been considered for the computation of load at ultimate stage.

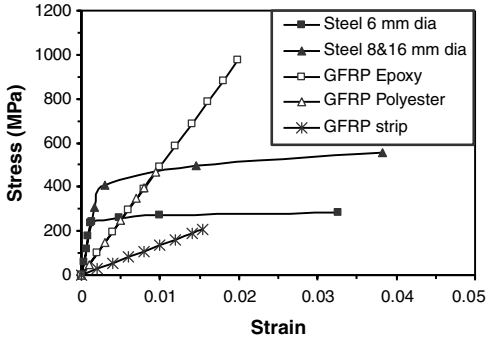

Fig. 7. Stress–strain characteristics of reinforcements.

The depth of neutral axis, x_u has been computed by an iterative technique based on the force equilibrium criteria given by Eq. (10)

$$\left| C_c + T_c + \sum_i F_{si} \right| \leqslant 0.01 \text{ kN} \tag{10}$$

Ultimate load carrying capacity of the section has been computed from the moment of resistance (M_u) using the beam geometry and has been given by Eq. (11).

$$P = 2(M_u/a) \tag{11}$$

$$M_u = C_c d_{cc} + T_c d_{ct} + \sum_i F_{si}(d_{si} - x_u) \tag{12}$$

'a' in Eq. (11) is the shear span of the beam. The moment of resistance of the section (M_u) in Eq. (11) has been computed by multiplying the component forces C_c, T_c and F_{si} with the corresponding distance of their line of action from the neutral axis, d_{cc}, d_{ct} and $(d_{si} - x_u)$, respectively as shown in Fig. 6. The first crack load has also been computed using the same iterative method by fixing the value of the strain in the extreme tensile fiber in the cross section as the cracking strain of the concrete matrix (ε_{ct} given by Eq. (4)).

The analytical model proposed in the present investigation is based on bending action of the beam. The present model is similar to the crack based analysis of single, straight shear crack accounting for only the dowel splitting of concrete along the reinforcement proposed by Stratford and Burgoyne [18]. In the proposed analytical model, only tensile stress in the rebar limited to the axial pullout of the rebar based on to the pullout test performed in this study has been considered (Eqs. (1) and (2)). Since the tests on beam did not indicate dowel rupture of the GFRP reinforcement, the same was not included in the proposed analysis.

3.2. Crack width prediction

A model has been proposed for predicting the maximum width of the crack (w) in the concrete beams reinforced with GFRP at various loading stages and has been given by Eq. (13). The proposed model for predicting the maximum crack width (w) has been derived from the model originally proposed by Tountanji and Saafi [19] incorporating modifications accounting for test data of the present study.

$$w = \frac{0.2}{E_{FRP}} (\rho_{FRP})^{-0.5} f_{si} \frac{(D - x_u)}{(d_{si} - x_u)} \sqrt[3]{d_c A_{ct}} \tag{13}$$

$$A_{ct} = \frac{2(D-d)b}{\text{number of bars}} \tag{14}$$

where E_{FRP} is the modulus of elasticity of FRP longitudinal reinforcements, ρ_{FRP} is the longitudinal reinforcement ratio of FRP reinforcements and f_{si} is the axial stress in the FRP bars located at a depth of d_{si}. For the beams with longitudinal tension reinforcements provided in multiple layers, stress in the bars closest to the tension face of the beam located at a depth equal to d_{s3} as shown in Fig. 6 has been taken as f_{si}. D is the overall depth of the section, x_u is the depth of neutral axis from the extreme compression fiber determined using the iterative procedure described earlier and d_c is the thickness of the concrete cover measured from extreme tension fiber to the center of closest layer of longitudinal bars. A_{ct} is the effective tension area of the concrete having the same centroid as that of the rebars in tension divided by number of longitudinal tension reinforcement and has been computed using Eq. (14). d is the effective depth of the cross section of the beam.

3.3. Deflection prediction

The prediction model of deflection given by Eq. (15) proposed by Razagpur et al. [7] has been employed to compute the deflection

$$\delta_{max} = \frac{PL^3}{48 E_c I_{cr}} \left[3\left(\frac{a}{L}\right) - 4\left(\frac{a}{L}\right)^3 - 8\eta\left(\frac{L_g}{L}\right)^3 \right] \tag{15}$$

$$\eta = \left(1 - \frac{I_{cr}}{I_g}\right) \tag{16}$$

where L is the clear span of the simply supported beam and E_c is computed using Eq. (8). I_{cr} is the moment of inertia of the cracked section about the neutral axis and has been computed based on the details given in Fig. 6. L_g is the uncracked length of the beam from the supports. As proposed by Razagpur et al. [7], η is computed using Eq. (16). I_g is the moment of inertia of the gross section about its centroidal axis.

4. Results and discussion

Ten concrete beams including three steel reinforced beams and seven GFRP reinforced beams were tested in the present experimental program. The ultimate flexural strength, crack width at various stages of loading and load–deflection performance of the beams have been predicted and compared with the experimental data.

4.1. Behavior of the test beams

In the initial stages of loading, for all the beams, cracks first appeared in the constant moment zone. As the load increased, additional cracks developed in the mid span and new vertical cracks formed in the shear span. With further increase in load in steel reinforced beams (FS1SOC, FS2SOC and FS2GFC), one of the flexural crack in the constant moment zone extended deep into the compression zone, reducing the area of concrete in compression leading to crushing of concrete. Hence, crushing of concrete was observed in beams reinforced with steel rebar at the ultimate stage of loading. The cracks developed in the test beams at the ultimate stage are given in Fig. 8. In the case of GFRP reinforced concrete beams, one of the vertical cracks in the shear span became critical and extended towards the loading point at the ultimate stage. These beams failed at a load lower than the design load and the failure was observed to be mainly due to the slip of the rebar from the surrounding concrete. The slipping of rebar in GFRP reinforced beams was indicated by splitting of concrete at the level parallel to the reinforcements shown in Fig. 8.

The load at first crack and at ultimate stage of loading is presented in Table 4. All the beams reinforced with the steel rebar failed in flexure approximately at an ultimate load close to the design load. The addition of polypropylene fibers at a maximum dosage (0.1% by weight of the cement) as recommended by the manufacturer was found to reduce the compressive strength of the concrete as could be seen in Table 1. The strength of polymer modified fiber reinforced concrete in Phase I (65 MPa concrete beam series) was found to be about 65% of the strength of corresponding ordinary concrete (Table 1). The cracking strength of the beams was observed to be varying with the compressive strength of the concrete. As the mechanism of failure in GFRP reinforced concrete beams was due to the slip of rebar, the ultimate strength was not much affected by the variation of concrete strength. In addition, debonding of the secondary surface deformations from the GFRP rebar surface was observed at ultimate stages of the loading. Accounting for this bond failure within the rebar, GFRP polyester binder based rebar having a tensile strength of 50% of the epoxy binder based GFRP rebar was used in the second phase. This prevented bond failure from controlling the design, as additional numbers of polyester binder based rebar were introduced to achieve the design moment capacity.

Figs. 9 and 10 show the crack width in the test beams at various loading stages. As seen in these figures, crack widths are higher in beams with GFRP rebars as compared to similar beams with steel rebars. This may be attributed to the significantly reduced stiffness of the GFRP reinforcement (same order as that of the concrete matrix).

Figs. 11 and 12 present the load deflection characteristics of the test beams of the present study. The load deflection plot indicated that for all the test beams the stiffness of the member at the initial stages of loading prior to the cracking is governed by the gross section properties of the member. The post cracking stiffness of all the beams were affected by the stiffness of the longitudinal reinforcements. As the steel rebar has greater stiffness and less slip with respect to the surrounding concrete matrix, steel reinforced beams showed a greater post cracking stiffness when

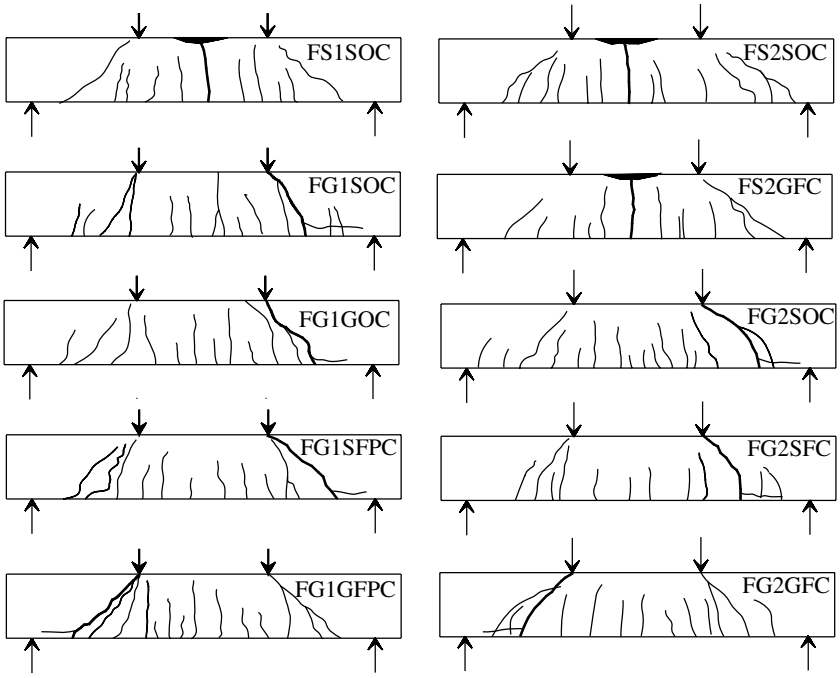

Fig. 8. Crack pattern in test beams at ultimate stage.

Table 4
Comparison of predicted load and experimental load of test beams

Sl. no.	Beam designation	Load at first crack			Load at ultimate		
		P_{cro} (kN)	P_{crp} (kN)	$\frac{P_{crp}}{P_{cro}}$	P_{uo} (kN)	P_{up} (kN)	$\frac{P_{up}}{P_{uo}}$
1	FS1SOC	72.85	–	–	299.20	–	–
2	FG1SOC	74.05	70.93	0.96	174.24	155.87	0.89
3	FG1GOC	71.75	68.59	0.96	168.96	155.62	0.92
4	FG1SFPC	59.55	56.28	0.94	163.08	153.89	0.94
5	FG1GFPC	55.46	52.17	0.94	161.92	153.02	0.95
6	FS2SOC	56.86	–	–	234.53	–	–
7	FS2GFC	51.92	–	–	221.10	–	–
8	FG2SOC	58.03	55.43	0.96	194.57	195.00	1.00
9	FG2SFC	56.35	52.77	0.94	187.33	194.00	1.04
10	FG2GFC	54.41	52.77	0.97	185.50	194.00	1.05
Average		–	–	0.95	–	–	0.97
Standard deviation		–	–	0.01	–	–	0.06

P_{cro} = Observed cracking load (experimental).
P_{crp} = Predicted cracking load (in Fig. 6 $x_{ct} = D$).
P_{uo} = Observed ultimate load (experimental).
P_{up} = Predicted ultimate load (in Fig. 6 $\varepsilon_{s3} = \varepsilon_{b\text{-}slip}$).

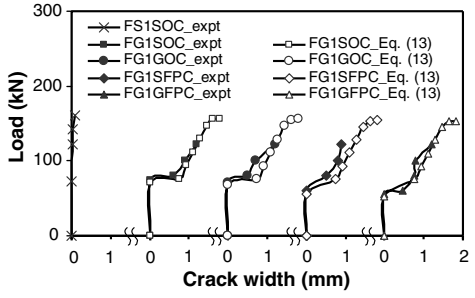

Fig. 9. Crack width in test beams of Phase I (65 MPa concrete beam series).

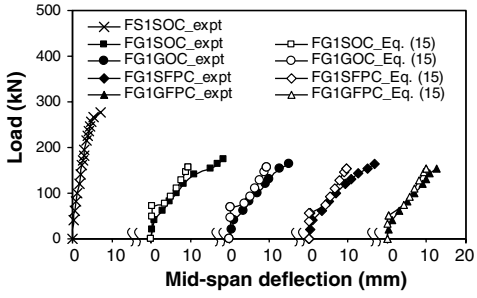

Fig. 11. Mid-span deflection of test beams in Phase I (65 MPa concrete beam series).

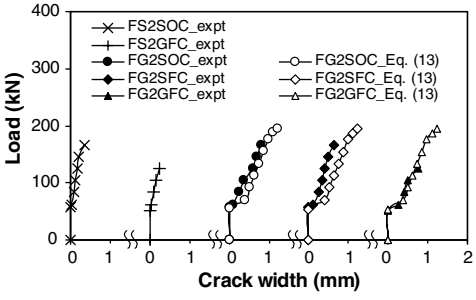

Fig. 10. Crack width in test beams of Phase II (35 MPa concrete beam series).

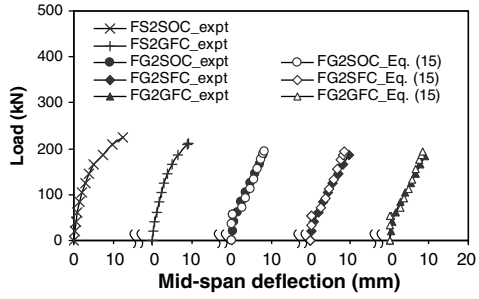

Fig. 12. Mid-span deflection of test beams in Phase II (35 MPa concrete beam series).

compared to the GFRP reinforced beams. The strain in the rebar at ultimate stage was found to be 0.004480, 0.004386 and 0.004495 for FS1SOC, FS2SOC and FS2GFC, respectively, indicating that yielding of longitudinal steel reinforcement ($\varepsilon_{sy} = 0.00429$) commenced very close to the ultimate stage. However, the LVDT instrumentations were removed before reaching to the expected ultimate stage loading, hence the post yielding plateau of the load deflection curve could not be captured in the steel reinforced test beams. However, due to the slipping of rebar from the concrete matrix, the GFRP reinforced beams show relatively less stiffness in the post cracking stage when compared to the steel reinforced beams. The effect of addition of polypropylene fibers on the post cracking behavior was observed to be marginal. On comparing the load deflection curves of FG1SOC with FG1GOC and FG2SOC and FG2GFC, it can be concluded that the GFRP stirrup reinforcements produced equal contribution in terms of force

sustained when compared to that of the steel stirrups in the post cracking stages of the GFRP reinforced beams. However, as GFRP stirrup material has substantially low stiffness when compared to the steel, the crack width in the shear span in the beams with GFRP stirrups was observed to be more when compared to that in the corresponding beams with steel stirrups. GFRP stirrup reinforcements produced equal contribution in terms of the force sustained as that of the steel stirrups in the post cracking stages in the GFRP reinforced beams. However, these stirrups are relatively less stiff and hence caused wider cracks in the shear span resulting in an early failure.

In the case of concrete beams reinforced with polyester based GFRP rebars (FG2SOC, FG2SFC and FG2GFC), the axial force developed in the bar at the failure of the beam due to the bond-slip mechanism was nearly 90% of the tensile strength. Hence, additional stirrups could possibly have lead to rupture of the polyester matrix based GFRP rebars. In the case of concrete beams reinforced with epoxy binder based GFRP rebar (FG1SOC, FG1GOC, FG1SFPC and FG1GFPC), the axial tensile forces mobilized in the bar at the failure of the beam was only 50% of its tensile strength. Thus, additional stirrups may not alter the observed failure mode in concrete beams reinforced with epoxy binder based GFRP rebar.

4.2. Comparison of analytical models

The load at ultimate stage of GFRP reinforced beams was predicted using the proposed model accounting for the slip between the rebar and concrete matrix at ultimate stage. The contribution of dowel action of the longitudinal rebar against the rotation of concrete block near to the support has been assumed to be negligible in the proposed model. The main force preventing the crack rotation is the force sustained by the longitudinal rebars. The slip along these bars leads to the failure of the beam. The load at first crack and the load at ultimate stage predicted using the proposed model has been compared with the experimental data in Table 4. The average value of the ratio of the predicted first crack load to the experimentally observed first crack load across all the GFRP reinforced beams was found to be 0.95 with a standard deviation of 1%. Similarly, the average value of the ratio of the predicted ultimate load to the actual ultimate load (observed in experiment) across all the GFRP reinforced beams was found to be 0.97 with a standard deviation of 0.06. This indicates that the present model can predict the load in GFRP reinforced beams at various stages of loading quite accurately.

Figs. 9 and 10 compares the predicted crack width of GFRP reinforced beams with the experimental data. It may be noted that the width of the crack in GFRP reinforced beams at various stages of loading has been reasonably predicted using the proposed model given by Eq. (13).

Figs. 11 and 12 compares the predicted load deflection characteristics of the GFRP reinforced beams with the experimental data. The comparison indicates that the proposed model given by Eq. (15) estimates the deflection of the GFRP reinforced beams at various stages reasonably well.

5. Conclusion

Based on the experiment and analytical investigation of GFRP reinforced beams, the following conclusions were derived:

1. Failure of the GFRP reinforced concrete beams was mainly due to its reduced post cracking stiffness and the slip between rebar and the concrete matrix.
2. Addition of polypropylene fibers had marginal effect on the post cracking behavior of the GFRP reinforced beams.
3. The proposed model accounting for the slip of the longitudinal reinforcements for predicting the strength of the GFRP reinforced beam predicted the load at different stages of loading quite accurately.
4. The crack width predicted using the proposed model for GFRP rebar reinforced beams given by Eq. (12) shows close agreement with the experimental data.
5. The load deflection response of the various GFRP reinforced beams have been predicted using Eq. (15) and seems to closely predict the corresponding experimentally observed response.

Acknowledgements

The authors wish to acknowledge the financial support received from the Department of Science and Technology, Government of India, New Delhi for carrying out this project (Grant No. II.3(3)/99-ET/9-11-2000).

References

[1] Nawy EG, Neuwerth GE. Fiberglass reinforced concrete slabs and beams. J Struct Div, ASCE 1977;103(ST2):421–40.
[2] Theriault M, Benmokrane B. Effect of FRP reinforcement ratio and concrete strength on flexural behavior of concrete beams. J Compos Constr, ASCE 1988;2(1):7–16.
[3] Saadatmanesh H, Ehsani MR. Fiber composite bars for reinforced construction. J Compos Mat 1991;25(2):188–203.
[4] Shapria A, Bank LC. Constructability and economics of FRP reinforced cages for concrete beams. J Compos Constr, ASCE 1997;1(3):82–9.
[5] Nanni A. Flexural behavior and design of RC members using FRP reinforcement. J Struct Engg, ASCE 1993;119(11):3344–55.
[6] Yost JR, Gross SP, Dinehart DW. Shear strength of normal strength concrete beams reinforced with deformed GFRP bars. J Compos Constr, ASCE 2001;5(4):268–75.
[7] Razaqpur AG, Svecova D, Cheung MS. Rational method for calculating deflection of fiber reinforced polymer reinforced beams. ACI Struct J 2000;97(1):175–84.
[8] Kumar LK, Ramaswamy A, Rao KSN. Behavior of reinforced SFRC beams in flexure and shear. In: Proceedings of the national conference on advances in civil engineering, Kharapur, India, 2002. p. 1151–7.

[9] CSA S806. Design and construction of building components with fiber reinforced polymers – S806-02. Canadian Standards Association, Rexdale, Ont, Canada, 2002.
[10] ACI 440. Guide for design and construction of concrete reinforced with FRP bars-ACI 440.1R-01. American Concrete Institute, Farmington Hills, Mich, 2001.
[11] JSCE. Recommendation for design and construction of concrete structures using continuous fiber reinforced materials. Tokyo: Japan Society of Civil Engineers; 1997.
[12] Sonobe Y, Fukuyama H, Okamoto T, Kani N, Kimura K, Kobayashi K, et al. Design guidelines of FRP reinforced concrete building structures. J Compos Constr, ASCE 1997;1(3):90–115.
[13] Xiao J, Li J, Zha Q. Experimental study on bond behavior between FRP and concrete. Constr Build Mat, ELSEVIER. 2004;18: 745–52.
[14] Orozco AL, Maji AK. Energy release in fiber reinforced plastic reinforced concrete beams. J Compos Constr, ASCE 2004;8(1):52–8.
[15] Thiagarajan G. Experimental and analytical behavior of carbon fiber based rods as flexural reinforcement. J Compos Constr, ASCE 2003;7(1):64–72.
[16] IS 456. Plain and Reinforced concrete-code of practice. Bureau of Indian Standards, New Delhi, India, 2000.
[17] Zhuang YP, Jiang JJ, Jing SY, Ye ZM. Basic elements of design for steel reinforced concrete structures. Beijing, China: Earthquake Press; 1990.
[18] Stratford TJ, Burgoyne CJ. Crack based analysis of concrete with brittle reinforcement. Mag Concr Res 2002;54(5):321–32.
[19] Tountanji HA, Saafi MM. Flexure Behavior of concrete beams reinforced with glass fiber-reinforced polymer (GFRP) bars. ACI Struct J 2000;97(5):712–9.